

Soft Touch using Soft Pneumatic Actuator–Skin as a Wearable Haptic Feedback Device

Harshal Arun Sonar, Jian-Lin Huang, and Jamie Paik*

Understanding the external environment depends heavily on vision, audition, and touch. Like vision and audition, the human sense of touch is complex. Tactile perception is composed of multiple fundamental and physical experiences felt as changes in stiffness, texture, shape, size, temperature, and weight by the skin. While researchers and industries have made continuous efforts to abstract and recreate these haptic experiences, haptic devices are still limited in invoking intricate and rich sensations. Herein, the design, model, and experimental validation of a wearable skin-like interface, able to recreate the roughness, shape, and size of a perceived object is presented; a platform for an interactive “physical” experience. The cogency of immersion through tactile feedback on moldable clay by the user response from the active haptic feedback, is examined. For the experimental test, a soft pneumatic actuator (SPA)-skin interface (90 Hz bandwidth) with a complex actuation pattern is prototyped. The SPA-skin’s performance using three sets of simulated textures ($<300\ \mu\text{m}$) and for reconstructing simulated contours (of a rectangle, circle, or trapezoid) in the virtual reality (VR) platform is investigated. The experimental results demonstrated for the first time how artificially created tactile feedback can indeed simulate physical interaction, with 83% average accuracy for contour reconstruction.

1. Introduction

Over the past decade, soft robotics research has focused on achieving safer and intuitive interactions using their compliant and inherently safe-to-operate soft (predominantly elastomeric-based) systems. There have been significant advances in the design, actuation, and control methods of this technology, opening up new avenues for wearable systems to provide improved task assistance and feedback for various applications.^[1–5] The capabilities of these soft, elastomeric material-based robots


allow further development of intimate human–robot interaction through haptic feedback.^[2,6]

Tactile feedback plays an important role in human–robot interaction. The human sense of touch, or tactile perception, consists of multiple experiences, which can be categorized as rough texture, fine texture, lateral friction, size, temperature, or weight.^[7–9] To successfully recreate a realistic feeling of touch in a virtual environment, a tactile feedback device should be able to integrate more than one of these multimodal sensations.^[9]

Researchers have characterized, modeled, and rendered tactile properties such as surface texture and hardness on tabletop interfaces.^[7,8,10] It is particularly challenging to develop a wearable tactile feedback device able to generate texture feedback, as this requires delivering a wide range of actuation frequencies. Mainly as the technological effort in wearable prototypes relied heavily on the use of vibrotactile electromechanical actuators, however, their localization capability and the range of actuation frequencies remain restricted. The use of voice coil actuators at the finger tips^[11–13] or the proximal phalanges^[14] helped improve the actuation range; however, this actuator solution is impractical in terms of size and weight needed to achieve a reasonable spatial resolution. Dielectric elastomer actuator (DEA)-based haptic devices combined with a wearable platform supply the much-needed mechanical compliance with human skin.^[15,16] However, they have a high voltage requirement and provide limited actuation forces in the range of 0.3–0.6 N. In conclusion, existing solutions for haptic feedback are compelling for a defined range of frequencies and forces in the preset format of a tabletop or for a few wearable platforms. However, currently there is no comprehensive solution or design that allows rendering a rich set of tactile feedback and actually verifies the effectiveness of this physical feedback, especially in a wearable format. In fact, what is lacking is a low-profile platform, thin enough to be mechanically transparent, which not only provides high-fidelity tactile feedback but also allows fingers to be free for simultaneous and instantaneous environmental exploration.

Similarly, translating a virtual object’s shape has been another principal focus of the haptic field. One way of recreating a shape is by actuating a 2.5D shape display, which consists of actuated pin arrays that can alter the heights of multiple pins in a grid.^[17–19] Some of these devices not only render the shape

H. A. Sonar, J.-L. Huang, Prof. J. Paik
Reconfigurable Robotics Laboratory
École Polytechnique Fédérale de Lausanne (EPFL)
1015 Lausanne, Switzerland
E-mail: jamie.paik@epfl.ch

 The ORCID identification number(s) for the author(s) of this article can be found under <https://doi.org/10.1002/aisy.202000168>.

© 2021 The Authors. Advanced Intelligent Systems published by Wiley-VCH GmbH. This is an open access article under the terms of the Creative Commons Attribution License, which permits use, distribution and reproduction in any medium, provided the original work is properly cited.

DOI: 10.1002/aisy.202000168

but further expand possibilities by integrating force control for the dynamic interpretation of force and stiffness of materials.^[20,21] Although these pin-based shape displays allow multipoint and multimodal cutaneous feedback for exploring virtual environments, the interactions are limited to a plane and a modulated height in the 2.5D experience. In addition, this type of shape display needs a large number of actuators (from 50 to several hundred), with a high aspect ratio (usually higher than 30) to map the shape of objects; this solution cannot be applied to a fully 3D environment. To generate shapes entirely in 3D, there are several interactive interfaces based on unconventional materials and actuators, such as soft pneumatic actuators (SPAs),^[22–24] jamming materials,^[25] or shape memory materials.^[26,27] Shape generation, however, is still restricted by the number of actuators, despite a few model-based designs achieving target shape with relatively small numbers of actuators.^[28,29] Some wearable/handheld devices^[12,13,30,31] provide an alternative solution for tangibly perceiving shapes and spatial information. They enable a more natural interaction and larger workspaces for shape exploration in contrast to tabletop devices, which have limited workspace.

In this article, we present for the first time the design of a comprehensive and coherent tactile information transfer system and an experimental protocol for validating the tactile feedback. Our approach utilizes a novel soft interactive interface linked to a soft malleable object. The soft interactive interface consists of an SPA layer integrated with a layer of piezoelectric lead–zirconate–titanate (PZT) sensors to form SPA–skin, providing a wide range of controlled vibratory feedback to the fingertips. The controlled feedback is able to generate texture and auxiliary tactile response, brought about by actuation frequencies being proportional to the distance from the target shape, therefore guiding users toward the intended shape. Then, association with a moldable test object (playdough) confirms, through its plastic deformation, the applied actuation forces of the user in response to the sensed feedback from the active interface. Together, this unique experimental setup and protocol produce tangible tactile feedback, and instant validation of its cogency in the user’s experience, of three different modes of tactile actuation: texture, size, and shape.

We explore the applicability of the SPA–skin as a tactile feedback device in a set of experiments that investigate a variety of haptic experiences, possible through the sensation of touch and tactile perception. The SPA–skin is first used to characterize macrotexture roughness using PZT sensors, followed by a frequency domain analysis, in which the texture is reconstructed using a pressure regulator, on–off valves, and SPAs. In a second experiment, we develop a testbed to reconstruct a virtual 2D shape using guided, multifrequency tactile feedback and active finger tracking. The participation of the user who actively acts on a moldable object closes the interaction loop, as the moldable object registers the intended 2D shape sensed by the user. This human-in-loop evaluation is critical for validating the tactile feedback at the interface and how well the human is integrated or immersed in the process. Here, the haptic feedback loop is closed through the user’s actions (**Figure 1b,c**), and the comparison between the moldable object’s final shape and the intended virtual shape is a measure of the effectiveness of the SPA–skin platform.

The major contributions of the presented work are as follows.

- 1) A novel testbed and protocol design to produce as well as experimentally quantify multimodal haptic feedback involving texture, size, and shape; 2) a unique PZT sensor-embedded SPA–skin and system design for high-bandwidth tactile feedback and noise isolation from soft grounds and dynamic interference; and 3) tactile cues to actively guide users for physical reconstruction planer shapes as a measure of the interaction response with the SPA–skin.

2. System Overview

Many of today’s virtual reality (VR) interfaces rely only on visual and auditory modes for the user interaction, limiting the user’s level of immersion due to lack of haptic feedback. Developing a human-in-loop interactive system requires realistic tactile feedback producing a range of tactile experiences, such as perception of shape, size, surface texture, and stiffness.^[8,32] Especially in the case of tactile exploration, texture and shape perception play inherent roles in gaining more information about the object being touched. Texture is perceived through the Meissner and Pacinian corpuscles (PCs), which can detect variations in roughness and texture while contacting the surface.^[8,33] The range of detection frequencies of Meissner, slowly adapting (SA)-type, and PCs, rapidly adapting (RA)-type is from 10–40 to 60–400 Hz, respectively, with maximum sensitivities around 30 and 250 Hz, respectively.^[8,33] As these frequencies demand a high-fidelity response from a device with appropriate actuation at the fingertips, only a few wearable platforms can currently render texture.^[8,11,31] Shape is the second fundamental property of an object necessary for human–computer interaction both for input and output devices. The ability to interact bidirectionally with shapes is essential for applications such as computer-aided design (CAD) and interactive digital fabrication.^[34,35] The tabletop shape displays provide possibilities for bidirectional interaction^[36,37] that make both perception and creation of shapes accessible, whereas most of the wearable/handheld haptic research have mainly focused on just perceiving the direction of shapes.

Another uninvestigated problem is the way to quantify spatial or textural accuracy of haptic stimuli in wearable devices, despite the well-studied precision of motion-tracking systems. There is some research examining the potential of digital shape recreation using wearable haptic devices in VR environments.^[38] However, the possibility of both perceiving and recreating shapes in a single human-in-the-loop integrated haptic system has rarely been considered or quantitatively evaluated. Closing the haptic feedback loop with human action triggered by tactile feedback would bring essential measures of applicability of the haptic feedback system and level of immersion. A platform, aware of human action and having active feedback control, could be coupled to quantitative analysis of the integrated system. To achieve the broad range of tactile perception frequencies and active feedback control, we propose a two-component system (**Figure 1**) consisting of an active wearable component and a passive soft and pliable test object to tackle the challenges of multimodal tactile exploration.

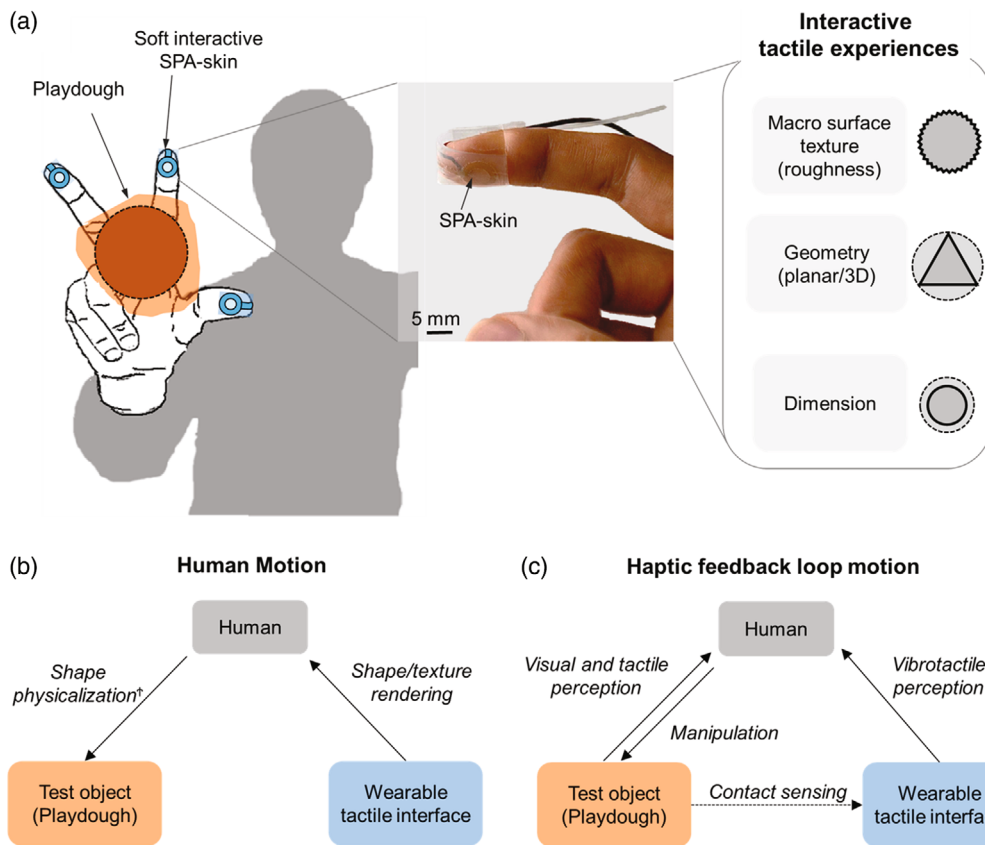


Figure 1. Wearable soft interactive interface. a) A two-component system combining a wearable interactive SPA-skin with a passive soft playdough object to generate the multiexperience tactile feedback of macrosurface textures, planar shapes, and size tracing. The SPA-skin interface is composed of an SPA actuation layer and a PZT sensing layer with 8 mm-diameter actuators and $2 \times 2 \text{ mm}^2$ PZT sensors. Integrated high-sensitivity (0.3 V N^{-1}) sensing allows closed-loop feedback control and simple texture classification. Multilevel tactile feedback is used for directed spatial localization of planar virtual shapes via a b) human motion side and c) haptic feedback-loop motion side. Human motion and haptic feedback-loop motion block diagrams illustrate the separate actions of the human and computer units. The wearable tactile interface triggers the human motion to help in physical shape rendering, “physicalization” (“Physicalization”: In this context, it is defined as the process of transferring the digital data to a physical/tangible form that people can explore and communicate with^[32]), of the moldable test object (b). The haptic feedback motion loop senses the location of the human fingers and the contact with the test object boundaries to generate multilevel tactile feedback (c).

2.1. Sensor-Actuator Bidirectional Interface Component

We used an “interactive SPA-skin” with integrated hi-fidelity actuation and sensing capabilities as the active component.^[39] The SPA-skin is a low-profile soft interface containing a PZT sensor layer, an SPA layer, and a controller controlling the SPA layer with a pneumatic regulator and high-speed on-off solenoid valves. The integrated sensing layer makes it possible to gather information about the local environmental loading conditions to modify the output required for coherent feedback. Together, the integrated sensing layer and an external finger tracking system provide bidirectional interaction between the SPA-skin and user.

2.2. Test Object Component

A second challenge for system design lies in producing a static force feedback, allowing a sense of touch. A virtual shape may be

perceived using a heavy and bulky electro-mechanical glove-like design but this has limited wearability. Here, we propose a test object made using playdough, which may be molded plastically into the desired shape according to the applied forces. Uniting the active interface and the test object provides coherent tactile feedback for an immersive experience.

While shape recognition could be augmented by a kinesthetic haptic device with passive haptic assistance, as discussed in a study by Rodriguez et al.,^[40] the integration of cutaneous sensation using playdough might be effective, as the spatial precision for macrofeatures of the objects mainly relies on SA1 afferents, which have a lower frequency of peak sensitivities. The playdough not only grants a response to perception of the shape, but also serves as an output device for quantitatively evaluating the spatial resolution via the human as an intermedium, as shown in Figure 1b. Playdough in fact serves as a means of “data physicalization,”^[41] a process transferring digital data to a physical/tangible form that people can explore and communicate with.

3. Experimental Evaluation and Protocol Design

Humans combine touching and physical exploration of an object to gain detailed information about the properties of the object being inspected. The surface exploration generates varying contour, hardness, and roughness profiles by dynamic shape exploration in space stimulating the particular mechanoreceptors. In this section, we developed a protocol to produce realistic tactile feeling and close the haptic loop with human interaction. For the first time we can validate tactile feedback in a physical manner. We used an SPA–skin interface granting actuation at required frequencies without losing on output amplitude combined with a human-in-loop exploration to generate a realistic feeling of two of the most important modes of dynamic explorations: texture and shape of a physical object recreated virtually.

3.1. SPA–Skin in Dynamic Conditions and Performance Characterization

The SPA–skin interface was designed to generate a wide range of vibrotactile stimulation, targeting the RA type-I and PC mechanoreceptors in the 10–100 Hz range.^[33] Many traditional devices use electromagnetic motors or voice coil actuators in the form of tabletop display or handheld displays to have a large actuation frequency range. However, they are limited to localized actuation and do not allow fingers to move freely in space to explore the environment as we naturally do. On the other hand, with SPA–skin, we can customize the actuator size, ranging from 2 mm diameter for acute location on areas like the finger tips to 20 mm diameter for low-sensitivity areas like the back of the neck.^[39] We selected 8 mm diameter ring-shaped SPAs for their high bandwidth, equal actuation area, and uniform inflation across the surface, as shown in **Figure 2b**. The ring-shaped actuator is powered through high-conductance solenoid valves (MHE2, Festo AG & Co. KG, Berkheim, Germany) improving the bandwidth from 35 to 129 Hz for the same SPA–skin thickness. We used Dragon Skin 30 (Smooth on Inc., USA) material to fabricate the SPA layers, which has a similar mechanical compliance to human skin (1–2 MPa) on fingers for transparent mechanical feedback.

3.2. Dynamic Characterization of the SPA Layer and PZT Sensor Layer

The SPAs were actuated over a wide spectrum of actuation frequencies, ranging from 0 to 120 Hz, producing 0.3 N static output blocked force under 0.1 N of initial static preload, to measure dynamic behavior (**Figure 2a,c**). The recorded frequency response is plotted for the SPA layer using a Nano-17 external 3D force sensor (ATI Industrial Automation, USA) and the SPA with a PZT sensor, measured from the PZT sensor (**Figure 2c**). A first-order transfer function (TF) fits well for the SPA–skin and the integrated PZT sensor dynamics, with R^2 values of 0.99 and 0.96, respectively, as given by Equation (1) and (2).

$$TF_{SPA} = \frac{0.332}{(0.00775 * S + 1)} N \quad (1)$$

$$TF_{SPA+PZT} = \frac{0.111}{(0.0116 * S + 1)} V \quad (2)$$

These TFs provide a combined sensor-actuator bandwidth of 86 Hz, measured through the PZT sensors, and 129 Hz for the SPA platform measured through the Nano-17 sensor. Even though the discrete PZT sensor with flexible electrodes has a relatively higher mechanical bandwidth due to a much higher stiffness (in GPa) than the SPA layer (1–2 MPa), the electrical properties of PZT sensors set the limit for the lower cutoff frequency of SPA–skin to 1.6–2.2 Hz (Supporting Information).

3.3. Controller for Human-in-Loop Dynamic Interactions

Humans explore with their fingers in lateral directions to understand the shape, size, hardness, and surface roughness usually at 10–80 mm s⁻¹ velocity.^[7,10,42] We tested the dynamic behavior of the finger to measure the lateral frictional forces produced with exploration velocities of 10 and 30 mm s⁻¹. The human finger produced a lateral friction of 0.25 N for a 1 N applied normal force when used with an artificial sinusoidal surface, fabricated with standard SLA material (**Figure 2d**). We then used a textured frictional cloth tape made of glass fiber (GL-96, Saint-Gobain performance plastics h-old S.p.A., Italy) to replace the human finger and replicate similar behavior in dynamic texture recording experimentally. This produced 0.3 N of lateral friction and a signature similar to that of the human finger in the tested frequency domain (**Figure 2d** and **Figure S1**, Supporting Information).

3.4. Texture Recording and Reconstruction Experiment

Experimental setups for reconstructing texture exist. However, as tabletop or handheld devices, they have a limited range of motion and often only provide texture feedback without shape exploration, due to the different interaction modes, and also lack the possibility of active touch.^[43] In active touch humans benefit from voluntary motor involvement that allows the user to generate various exploratory patterns tailored to each tactile property for improved perception of the surface.^[7,43,44] SPA–skin offers a compliant, low-profile wearable platform, leaving hands and fingers free for doing their usual activity. We decided to use the wide bandwidth of SPA–skin along with the possibility of active tactile exploration intact, to generate a realistic tactile feedback. For the experimental design, we chose three simple sinusoidal shapes with no gap, a single gap, or a double gap between two consecutive sine waves. The surface roughness height (h) was selected as 300 μm^[45] (**Figure 2d**), as it lies in the range of rough texture that can be felt on static pressing, but still requires human fingers to explore it laterally.^[7,42,46] Also, when subjected to 10–50 mm s⁻¹ exploration tests, it will naturally generate the fundamental frequencies of 2–50 Hz, well within the range of the SPA–skin’s performance, at a spatial wavelength (λ) of 1.5 mm (**Figure 2d**).

A control algorithm using a fast Fourier analysis and detection of peaks from the spectral graph allowed discrete generation of the required waveform at an approximate level. The currently available pressure regulators have a very limited bandwidth of less than 3 Hz due to integrated proportional–integral–derivative

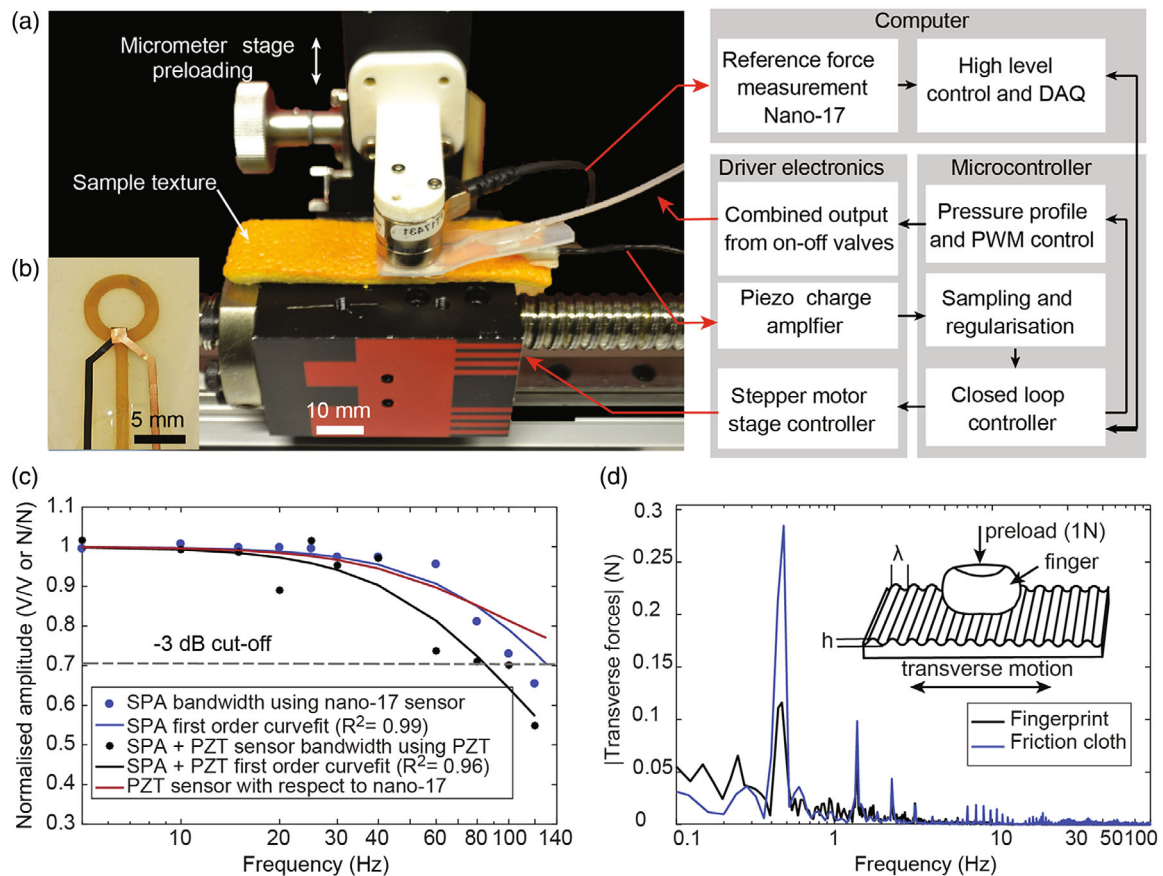


Figure 2. Dynamic characteristics of SPA-skin. a) Block diagram of the system characterization setup to record and render texture and dynamic characterization of the SPA-skin. The micrometer stage allows constant preloading. An orange peel of $10 \times 50 \text{ mm}^2$ was used as the test texture. b) SPA-skin prototype with 8 mm-diameter SPA and 2 mm channel width and a $2 \times 2 \text{ mm}^2$ PZT sensor placed at the intersection of the ring with inlet channel, where maximum inflation occurs. c) SPA, PZT sensor, and the combined integrated sensor-actuator bandwidth were measured using an external Nano-17 sensor and PZT sensor. The first-order transfer function fit provides 86 and 129 Hz with the sensor combined and independent bandwidth of the SPA, respectively. d) A comparison of frequency components observed with the human finger and friction cloth tape of $10 \times 10 \text{ mm}^2$, while recording the transverse forces generated with 1 N preload against a plain 3D-printed PLA material ($h = 0 \text{ mm}$). The human finger produced an average of 0.25 N lateral force, whereas the friction cloth tape produced 0.3 N for similar loading conditions.

controllers and higher-solenoid inertia (ITV1011, SMC Corporation, USA). To recreate the recorded spectrum, we therefore combined output from two on-off solenoid valves, tuned to the required spectral frequencies (Figure S1b, Supporting Information). The difference in actuation amplitude was controlled using the duty cycle of valve actuation and the overall average output force by controlling the pressure globally through the low-bandwidth regulator. The added capabilities of faster regulatory options (like a piezopressure regulator) allow covering much wider spectral signals. The signals lying at a higher frequency than the bandwidth of the regulator may be controlled using on-off valves actuated at the principle frequency components.

3.5. Shape Reconstruction Experiment

The shape perception is especially challenging for wearable devices due to the multimodality of cutaneous sensation in bidirectional interaction, involving active exploration of the object's

surface linked to intended motion coupling (sensory-motor coupling). The sense of shape relies on both SA1 and RA type afferents,^[8,33] where their individual perceptions have varied peak sensitivity frequencies, which is challenging to integrate into a single wearable haptic system. Also, most of the current haptic research is focused on creating perceptions and qualitatively evaluating the feeling by haptic devices. In fact, quantitative studies of the perception received and how humans respond are rare; it is especially challenging to quantify performance with human in the loop; human behavior is not usually reproducible and is difficult to measure. Here, we propose a test protocol and quantify shape sensation at the fingers.

The objective of the experiment is to evaluate the capacity of the active interactive interface to deliver spatial information sensations of virtual objects in terms of shape and size to the user who simultaneously physicalizes the sensations via the test object. We used vibrotactile feedback through SPA-skin as the active interactive interface and playdough as the test object, as shown in Figure 1b,c. When integrated seamlessly, we would

be able to achieve an immersive interactive tactile VR experience (Figure 3c).

The assumption for the experiment is that the active exploration of shapes and concurrent hand motion control shaping of the playdough can be achieved using the SPA–skin due to its soft material properties and broad vibration frequency bandwidth; the rigidity of other wearable devices might be an obstacle for exploring and creating virtual shapes. We also presume that playdough can be a base for shape sensation in active exploring, and the effectiveness is comparable with other wearable devices having kinesthetic feedback assistance.^[12]

The experimental setup is shown in Figure 3. The proposed task was to shape the playdough to match predefined geometries, guided only by the vibrotactile feedback through the SPA–skin and feel of the playdough. There was no visual feedback or shape contour information. The target shapes were limited to 2D contours instead of 3D geometries to simplify the task, cancel undesired noise, and relieve workload. The playdough was placed on a smooth transparent glass platform. A camera was installed underneath the glass platform to track colored markers attached to the fingers. The sampling rate of finger position was 10 Hz. The captured images provided spatial information, allowing tactile sensation of the virtual objects by the SPA–skin in real space. The SPA–skin vibrated when the fingers approached or reached the 2D contour of the virtual object. Then, the 2D contour of the

virtual object was recreated physically, manipulating the playdough. Finally, the trajectories of fingers and the final contours of the playdough were recorded to examine the effectiveness of spatial information delivery.

We defined three different target contours: rectangle, trapezoid, and circle, to provide flat lines, inclined lines, and curves with respect to the grasping motion of the fingers. We gave one target contour per test. The target contours were relatively simple without detailed features or concave lines, designed mainly to promote simple grasping gestures, avoiding complex manipulation and thereby, interference from other factors. Furthermore, there were two horizontal cuts on the glass as boundaries to the shape generation motion, as shown in Figure 3. With the boundary constraint, shaping progress was focused on grasping motion control and tactile perception of the fingers, without larger movements of entire hands or arms. The shaping process lasted 2 min per test. Nine tests for each target contour were conducted on three subjects whose age ranged from 28 to 34 years.

4. Results and Discussion

SPA–skin delivered a wide range of modulation experiences proven by dynamic characterization. Coupling the SPA–skin to a texture-reconstruction testbed or to a camera-monitored test

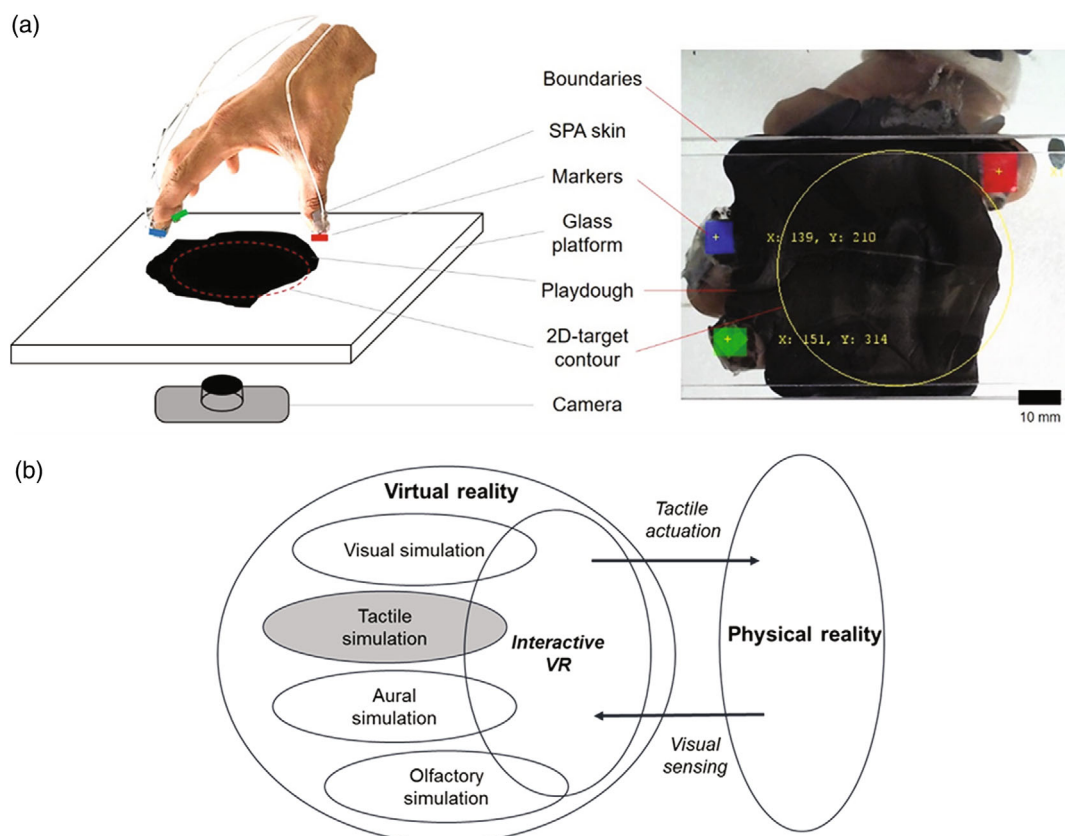


Figure 3. a) Experimental setup for interactive shape generation using SPA–skin and a playdough as a test object. The image on the right is the computer vision of the control system. b) SPA–skin setup with tactile actuation and visual sensing closing the loop with tactile simulation, a part of interactive VR environment and physical reality.

object produced experimental results that validated, for the first time, how an artificially created tactile feedback could indeed simulate physical interaction. Furthermore, the two devised experiments showed that the SPA–skin platform facilitated transfer of rich tactile information from virtual objects, such as surface roughness, dimension, and shape. Shape information could be reconstructed by transferring a virtual experience effectively to a physical one.

4.1. Texture Reconstruction Experiment

To have a realistic measure of texture feedback we devised a frequency-based approach, where principle components of frequencies were selected and generated using on–off solenoid valves, which have bandwidth in excess of 100 Hz (Figure 2c). This approach allowed control of the principle frequency components: as the spatial exploration velocity (v) changes, the actuation frequency changes linearly ($f = v/\lambda$). With the current experimental setup, we could integrate discrete output from two principle frequency components and their natural harmonics.

We preloaded the friction fabric-coated SPA–skin at 0.1 N and recorded the blocked force using PZT sensors and a Nano-17 sensor at 10 kS s^{-1} for three sets of waveforms (Figure 4a). With a 1.5 mm spatial wavelength, we observed a principle frequency component at 2.3 Hz for 10 mm s^{-1} exploration speed and 6.9 Hz for 30 mm s^{-1} exploration speed. We set the SPA

actuation frequency to 2.3 Hz and regulator pressure to have a similar 0.3 N average output, which showed a successful reconstruction of the recorded amplitude spectrum of the actual texture (Figure 4a).

In the last set of experiments, we used a $10 \times 50 \text{ mm}^2$ piece of orange peel with $\approx 2 \text{ mm}$ spatial indentations as the textured surface and recorded the forces using the PZT and Nano-17 force sensors. The frequency domain measurements showed two peak frequencies at 9.7 and 10.6 Hz. On reconstruction we observed a very similar frequency spectrum to the SPA–skin (Figure 4b). These frequencies also held for the generation of a slow moving tone of 0.9 Hz, which had an organic feeling, similar to soft-surface exploration.

4.2. Shape Reconstruction Experiment

To evaluate the spatial accuracy and effectiveness of the tactile exploration, the final contour of the playdough after the shaping process was compared with the target contour, as shown in Figure 1b. The accuracy of the shaping process was defined as the correlation coefficient of the area. The finger trajectory shaping process was recorded and the sets of experimental results are shown overlapping in Figure 5a, for multiple test subjects and for three shapes and sizes. The temporal exploration by the human fingers during the reconstruction process is shown in Figure 5b. The two red dashed lines are boundaries limiting

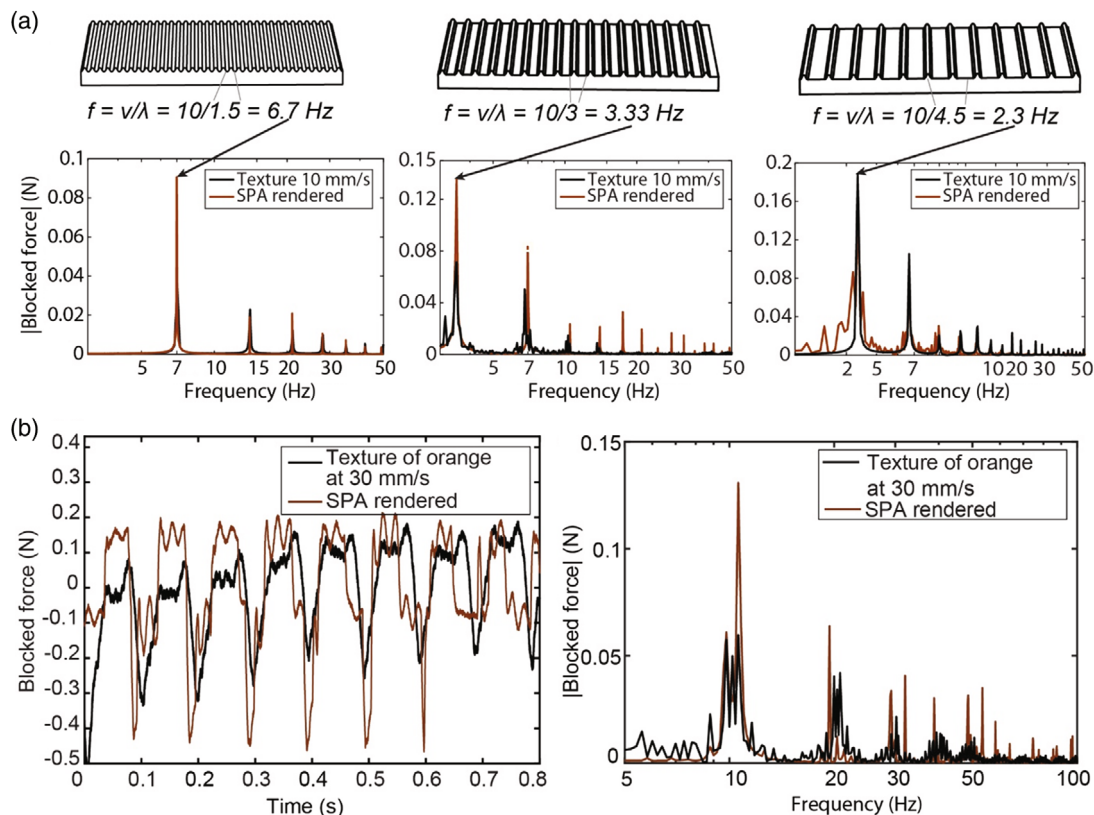


Figure 4. Texture reconstruction experimental results. a) Frequency response of three different sinusoidal textures recorded at 10 mm s^{-1} exploration velocity and texture rendering using the SPA–skin. b) A phase-matched time domain response and frequency components of fresh orange peel texture recorded at 30 mm s^{-1} compared with the rendered texture using the SPA skin at 0.3 N peak-to-peak blocked force.

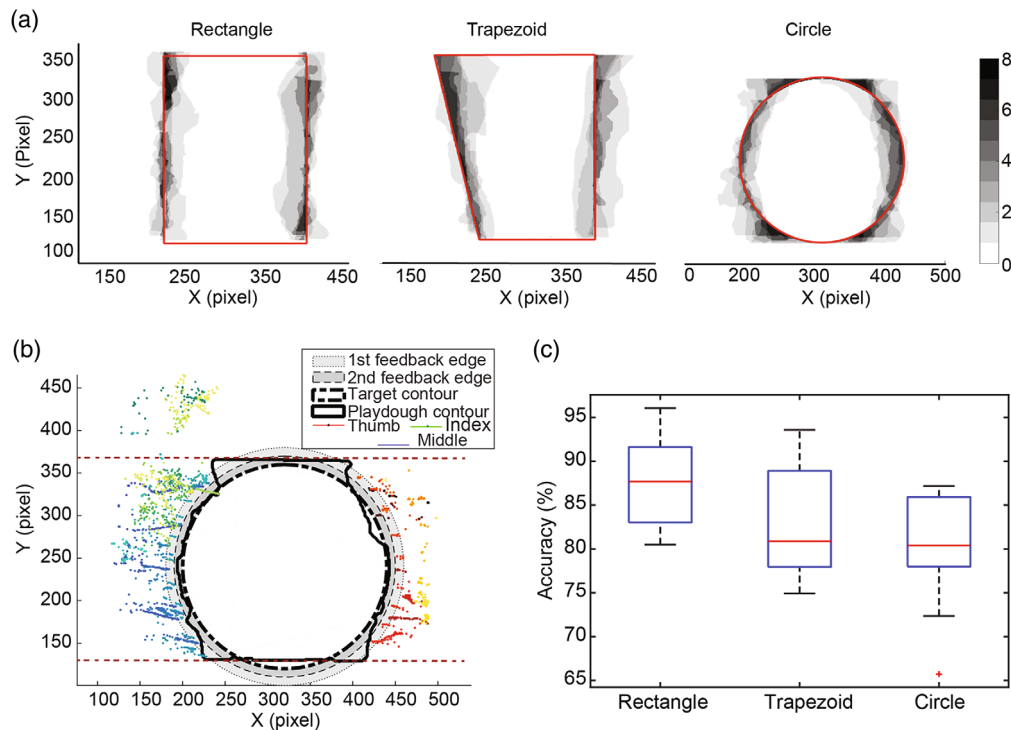


Figure 5. Results of the shape reconstruction experiments. a) Intensity map of the shape difference between the playdough shape and target shape. The error intensity mapping for the shape reconstruction experiments for three target shapes: rectangle, trapezoid, and circle. The darkest color represents the higher trends of error distributed in the 2D plane. The red line is the target contour. b) The finger trajectory shaping process and the comparison between target and playdough contours. The different feedback frequencies acknowledging approaching the target contour or reaching the target contour are shown as different shaded areas. The two horizontal red dashed lines are the boundaries limiting the workspace of the grasping motion. c) Calculated average area accuracy of shape reconstruction.

the workspace of the shaping process. The playdough contour, outside of the workspace, is removed in the figure for the accuracy calculation. The colored dots from light to dark represent the finger center locations from the start to the end of one set of experiments. There are three concentric circles, representing the boundaries of the first feedback edge, second feedback edge, and the target contour, respectively. The first and second feedback edges were defined as 20 pixels and 10 pixels from the target, respectively, as shown in Figure 5b. The control system gave a 15 Hz vibrotactile signal, signifying the approach of the target contour when the fingers reached the first feedback edge. A higher 35 Hz frequency signal was generated on the SPA-skin to give the sensation that fingers were really touching the boundary of the target shape when the finger center reached the second feedback edge. As mentioned previously, both SA1 and RA afferents are relevant in grasping control. The vibration frequency of the second feedback edge was close to the frequency of peak sensitivity for RA afferents and could be an effective stimulus for grasping control. The ten-pixel distance from the target contour was the definition as we roughly defined a 6 mm thickness for fingertips and one pixel equaled 0.29 mm in the region of interest. In Figure 5b, most of the finger-tracking points are located between the first and second feedback edges and only a few of them between the target and second feedback edge. It shows that the system gave an effective vibrotactile signal for acknowledging the appearance of virtual boundaries.

The contact forces from grasping the playdough were also present at the same time in this case.

Horizontal grasping motions were frequently used to shape the playdough, observed by the trajectories of fingers in Figure 5b. Thus, the spatial accuracy of the grasping motion could also be evaluated by calculating the area difference as the area is the horizontal difference integral along the y -axis. The calculated accuracy of all data sets is shown in Figure 5c and the image processing for accuracy comparison in Figure S2, Supporting Information. We achieved almost 90% accuracy for the rectangle contour and almost 80% accuracy for the circle contour using vibrotactile feedback. The circle contour had a lower average accuracy and we also saw a possible outlier for the circle case. A suggested reason for the lower accuracy could be the stop of airflow in the SPA-skin due to the large bending on the rubber tube, which led to a lower-amplitude vibrotactile feedback.

To investigate the effectiveness of the proposed SPA-skin feedback system in grasping control, we studied the distribution of the error area to find the ratio of the error area inside the target boundary to that outside the boundary and the image processing, as shown in Figure 5a and Figure S2d, Supporting Information. The error distribution showed that there was no significant difference between the error inside the target boundary (8.5%) or outside the boundary (7.8%), which suggested that the vibrotactile feedback from the SPA-skin is effective for grasping control.

To further examine if outside factors had a significant effect on accuracy, we performed one-way analysis of variance (ANOVA) tests^[47] on the target shapes, participants, and test order (divided into three groups: tests 1–3, tests 4–6, and tests 7–9). In these cases, F critical value $F_{crit} = 3.4$ at $\alpha = 0.05$. The F ratios were 3.2, 2.3, and 0.4, respectively, namely $F_{crit} > F$ ratio; hence, the results showed that none of the factors had a significant effect on the accuracy with a 95% confidence interval. The influence of the tested shapes on accuracy was minor; however, the contours tested were designed for rough geometries without detailed features, mostly composed of straight lines and uniform curvature lines. The accuracy of reconstructed shapes with detailed features with respect to dimension and geometry of the fingertips could be further studied. In addition, we observed that the learning factor was not significant in ANOVA tests of test order. Further studies could be done with more sets of experiments and changing the design of the test-shape order to examine learning factor influence on the same shape, as the current test shapes were hidden, picked at random before each test.

5. Experimental Section

5.1. SPA Layer Design and Fabrication

SPA-skin also has high flexibility in actuator design; for our application on fingers, a ring shape was chosen for a higher bandwidth of actuation for the same area and a uniform inflation profile across the surface without compromising on the blocked force (1 N at 50 kPa).^[48] A 400 μm -thick layer of Dragon skin 30 was fabricated using a thin-film applicator (ZAA2300, Zeihntner GmbH, Germany) upon which a laser-cut masking layer was carefully applied. This layer was then encapsulated using a final 400 μm top layer of silicone. The masking layer was created using a laser-cut polypropylene tape with selected shape for the actuator. For wearability at the fingertip, we selected an SPA of 8 mm diameter and a 2 mm channel for the mask (Figure 2), which achieved a bandwidth of 129 Hz with the current setup, with a 1 m tube length and 1.5 mm I.D. at a constant pressure of 50 kPa input and 0.1 N preload.

5.2. PZT Sensor Design and Fabrication

We selected PZT (PZT5H, CeramTec GmbH, Germany) discrete sensors due to their dynamic response, active sensing, and high sensitivity in detecting low-amplitude high-frequency vibrations.^[39] The sensing layer was integrated as a thin layer of silicone (100 μm) into the SPA layer (800 μm) that helps form a monolithic sensor-actuator structure, which is flexible in one direction and stretchable in the other, suitable to be worn on fingers (Figure 2b). The PZT sensor was placed at the intersection of the inlet channel and the ring-shaped SPA for minimal disturbance from inflation during external loading.

However, PZT sensors are rigid with flexible electrodes having a relatively higher mechanical bandwidth due to their much-higher stiffness than the SPA layer; hence, the electrical properties of PZT sensors limit the lower cutoff frequency over the mechanical properties. We manufactured a batch of five PZT

sensors for this experiment, which resulted in a lower cutoff frequency ranging from 1.6 to 2.3 Hz as a result of the electrical properties of the PZT sensor ($R = 180\text{--}250\text{ k}\Omega$ and $C = 750\text{--}800\text{ nF}$). At the same time, the electronic charge amplifier used for signal conditioning did not limit the upper cutoff frequency but the silicone material of SPA layer did, which is still higher than SPA-skin actuation bandwidth (Figure 2c).

The experiments involving human subject have been performed with the full, informed consent of the user.

6. Conclusion

For an effective wearable haptic feedback device, we require an accurate understanding of the physical interactions between the device and the wearer's perception. We propose a two-component system to achieve a multiexperience tactile feedback and, for the first time, human-in-loop "physical" validation of user actions, closing the haptic feedback loop. We use SPA-skin for its low-profile form factor, high-bandwidth capabilities, and integrated sensing as an active bidirectional interface. Special design measures in PZT sensor signal conditioning like high-sensitivity instrumentation amplifiers with noise filtering using coaxial cables and line noise notch filters allow for on-body placement and accurate measurements.

In the first stage, we designed and validated abilities of the SPA-skin interface to record a set of sinusoidal textures with similar indentations but different spatial resolution, which then were analyzed for the principle frequencies in the Fourier domain. The SPAs were then used to recreate the texture feedback approximately. It was seen that the natural textures also had a range of harmonics similar to what we obtained with the on-off nature of the SPA actuations. We recreated the natural texture of the orange peel with two principle frequency components with cross-correlation of 59% explored at 30 mm s^{-1} . These texture patterns once recorded could be shifted linearly in actuation frequencies, based on the real-time exploration velocity, making it an immersive experience for the human.

We then designed and validated a haptic system in which the delivery of tactile feedback and spatial accuracy was quantitatively studied for the bidirectional human-in-the-loop system. A 2D planer platform was used to "physicalize" a given virtual shape using a soft test object based on two-level tactile cues guiding human actions. The test object playdough, on being molded, provided the sense of shape and size whereas active tactile feedback from SPA-skin overlaid the texture cues. The results showed almost 90% accuracy for the rectangular shape- and greater than 80% for the trapezoidal- and circular-shape physicalization using SPA-skin for tactile guidance. We used two-stage actuation with low-frequency stimulation when approaching the contour shape, followed by a high-frequency vibration, when reaching the actual contour for ease of exploration.

The two experiments showed that SPA-skin is an effective haptic platform and provided rich tactile feedback in a wearable scenario. The tactile feedback loop was closed with human actions and was quantitatively validated for the level of immersion and quality of tactile feedback. There is plenty of room for further studies of multimodal perception with wearable soft haptic devices due to the customizability of both material properties

and control frequencies. These preliminary studies open up discussion for the next generation of haptic feedback devices, which are not only mechanically transparent for human wearability but also provide ranges of tactile sensations inherent to the object and perceived by the human sense of touch.

Supporting Information

Supporting Information is available from the Wiley Online Library or from the author.

Acknowledgements

This work was funded by the Swiss National Science Foundation (SNSF) through the National Centre of Competence in Research (NCCR) in Robotics.

Conflict of Interest

The authors declare no conflict of interest.

Keywords

human–robot interactions, multimodal haptic feedback, soft actuators, vibrotactile feedback

Received: July 23, 2020

Revised: November 9, 2020

Published online: January 25, 2021

- [1] Y. Yang, Y. Wu, C. Li, X. Yang, W. Chen, *Adv. Intell. Syst.* **2020**, *2*, 1900077.
- [2] A. T. Asbeck, S. M. M. D. Rossi, I. Galiana, Y. Ding, C. J. Walsh, *IEEE Robot. Autom. Mag.* **2014**, *21*, 22.
- [3] M. Cianchetti, C. Laschi, A. Menciasci, P. Dario, *Nat. Rev. Mater.* **2018**, *3*, 143.
- [4] D. Rus, M. T. Tolley, *Nature* **2015**, *521*, 467.
- [5] G. Agarwal, M. A. Robertson, H. Sonar, J. Paik, *Sci. Rep.* **2017**, *7*, 14391.
- [6] A. T. Maereg, A. Nagar, D. Reid, E. L. Secco, *Front. Robot. AI* **2017**, *4*, 42.
- [7] R. L. Klatzky, S. J. Lederman, C. Reed, *J. Exp. Psychol.: Gen.* **1987**, *116*, 356.
- [8] S. Okamoto, H. Nagano, Y. Yamada, *IEEE Trans. Haptics* **2013**, *6*, 81.
- [9] D. Wang, K. Ohnishi, W. Xu, *IEEE Trans. Ind. Electron.* **2020**, *67*, 610.
- [10] T. Yoshioka, J. Zhou, *Adv. Robot.* **2009**, *23*, 747.
- [11] S. B. Schorr, A. M. Okamura, in *Proc. of the 2017 CHI Conf. on Human Factors in Computing Systems*, Association For Computing Machinery, Denver, Colorado **2017**, pp. 3115–3119.
- [12] M. Gabardi, M. Solazzi, D. Leonardis, A. Frisoli, in *2016 IEEE Haptics Symposium (HAPTICS)*, Philadelphia, PA **2016**, pp. 140–146.
- [13] F. Chinello, M. Malvezzi, C. Pacchierotti, D. Prattichizzo, in *2012 IEEE Haptics Symposium (HAPTICS)*, Vancouver, BC **2012**, pp. 71–76.
- [14] X. de Tinguy, C. Pacchierotti, M. Marchal, A. Lecuyer, in *2018 IEEE Conf. on Virtual Reality and 3D User Interfaces (VR)*, IEEE, Reutlingen **2018**, pp. 81–90.
- [15] G. Frediani, H. Boys, S. Poslad, F. Carpi, in *Haptics: Perception, Devices, Control, and Applications*, Springer, Cham **2016**, pp. 326–334.
- [16] H. Zhao, A. M. Hussain, A. Israr, D. M. Vogt, M. Duduta, D. R. Clarke, R. J. Wood, *Soft Robot.* **2020**.
- [17] F. Vidal-Verdu, M. Hafez, *IEEE Trans. Neural Syst. Rehabil. Eng.* **2007**, *15*, 119.
- [18] S. Follmer, D. Leithinger, A. Olwal, A. Hogge, H. Ishii, in *Proc. of the 26th Annual ACM Symp. on User Interface Software and Technology – UIST '13*, ACM Press, St. Andrews, Scotland **2013**, pp. 417–426.
- [19] D. Leithinger, D. Lakatos, A. DeVincenzi, M. Blackshaw, H. Ishii, in *Proc. of the 24th Annual ACM Symp. on User Interface Software and Technology*, Association For Computing Machinery, New York, NY **2011**, pp. 541–548.
- [20] K. Nakagaki, L. Vink, J. Counts, D. Windham, D. Leithinger, S. Follmer, H. Ishii, in *Proc. of the 2016 CHI Conf. on Human Factors in Computing Systems*, ACM, San Jose, California **2016**, pp. 2764–2772.
- [21] K. Nakagaki, D. Fitzgerald, Z. (John) Ma, L. Vink, D. Levine, H. Ishii, in *Proc. of the Thirteenth Int. Conf. on Tangible, Embedded, and Embodied Interaction*, ACM, Tempe, Arizona **2019**, pp. 615–623.
- [22] L. Yao, R. Niiyama, J. Ou, S. Follmer, C. Della Silva, H. Ishii, in *Proc. of the 26th Annual ACM Symp. on User Interface Software and Technology – UIST '13*, ACM Press, St. Andrews, Scotland **2013**, pp. 13–22.
- [23] J. Ou, M. Skouras, N. Vlavianos, F. Heibeck, C.-Y. Cheng, J. Peters, H. Ishii, in *Proc. of the 29th Annual Symp. on User Interface Software and Technology*, ACM, Tokyo, Japan **2016**, pp. 121–132.
- [24] N. Takizawa, H. Yano, H. Iwata, Y. Oshiro, N. Ohkohchi, *IEEE Trans. Haptics* **2017**, *10*, 500.
- [25] S. Follmer, D. Leithinger, A. Olwal, N. Cheng, H. Ishii, in *Proc. of the 25th Annual ACM Symp. on User Interface Software and Technology*, ACM, New York, NY, USA **2012**, pp. 519–528.
- [26] A. Roudaut, A. Karnik, M. Löchtefeld, S. Subramanian, in *Proc. of the SIGCHI Conf. on Human Factors in Computing Systems*, ACM, New York, NY, USA **2013**, pp. 593–602.
- [27] J.-L. Huang, Z. Zhakypov, H. Sonar, J. Paik, *Int. J. Robot. Res.* **2018**, *37*, 629.
- [28] L.-K. Ma, Y. Zhang, Y. Liu, K. Zhou, X. Tong, *ACM Trans. Graphics* **2017**, *36*, 1.
- [29] M. Koehler, N. S. Usevitch, A. M. Okamura, *IEEE Trans. Robot.* **2020**, *36*, 613.
- [30] F. Chinello, M. Malvezzi, D. Prattichizzo, C. Pacchierotti, *IEEE Trans. Ind. Electron.* **2020**, *67*, 706.
- [31] H. Benko, C. Holz, M. Sinclair, E. Ofek, in *Proc. of the 29th Annual Symp. on User Interface Software and Technology*, ACM, Tokyo **2016**, pp. 717–728.
- [32] F. Chinello, M. Malvezzi, C. Pacchierotti, D. Prattichizzo, in *2012 IEEE Haptics Symp. (HAPTICS)* **2012**, pp. 71–76.
- [33] S. Choi, K. J. Kuchenbecker, *Proc. IEEE* **2013**, *101*, 2093.
- [34] C. Weichel, J. Hardy, J. Alexander, H. Gellersen, in *Proc. of the 28th Annual ACM Symp. on User Interface Software & Technology – UIST '15*, ACM Press, Daegu, Kyungpook **2015**, pp. 93–102.
- [35] S. Mueller, A. Seufert, H. Peng, R. Kovacs, K. Reuss, F. Guimbretière, P. Baudisch, in *Proc. of the Thirteenth Int. Conf. on Tangible, Embedded, and Embodied Interaction*, ACM, Tempe, Arizona **2019**, pp. 315–323.
- [36] D. Leithinger, S. Follmer, A. Olwal, H. Ishii, in *Proc. of the 27th Annual ACM Symp. on User Interface Software and Technology – UIST '14*, ACM Press, Honolulu, Hawaii **2014**, pp. 461–470.
- [37] A. F. Siu, J. Miele, S. Follmer, in *Proc. of the 20th Int. ACM SIGACCESS Conf. on Computers and Accessibility*, ACM, Galway, Ireland **2018**, pp. 343–345.
- [38] Z. Gao, H. Wang, G. Feng, F. Guo, H. Lv, B. Li, *Multimed. Tools Appl.* **2019**, *78*, 26569.
- [39] H. A. Sonar, J. Paik, *Front. Robot. AI* **2016**, *2*, 38.
- [40] J.-L. Rodríguez, R. Velázquez, C. Del-Valle-Soto, S. Gutiérrez, J. Varona, J. Enríquez-Zarate, *Electronics* **2019**, *8*, 355.

- [41] Y. Jansen, P. Dragicevic, P. Isenberg, J. Alexander, A. Karnik, J. Kildal, S. Subramanian, K. Hornbæk, in *Proc. of the 33rd Annual ACM Conf. on Human Factors in Computing Systems*, Association For Computing Machinery, Seoul **2015**, pp. 3227–3236.
- [42] A. I. Weber, H. P. Saal, J. D. Lieber, J.-W. Cheng, L. R. Manfredi, J. F. Dammann, S. J. Bensmaia, *Proc. Natl. Acad. Sci.* **2013**, *110*, 17107.
- [43] T. Yoshioka, J. C. Craig, G. C. Beck, S. S. Hsiao, *J. Neurosci.* **2011**, *31*, 17603.
- [44] S. J. Lederman, R. L. Klatzky, *Cognit. Psychol.* **1987**, *19*, 342.
- [45] M. Hollins, S. R. Risner, *Percept. Psychophys.* **2000**, *62*, 695.
- [46] A. M. Smith, G. Gosselin, B. Houde, *Exp. Brain Res.* **2002**, *147*, 209.
- [47] L. Sthle, S. Wold, *Chemom. Intell. Lab. Syst.* **1989**, *6*, 259.
- [48] A.-M. Georganakis, H. A. Sonar, M. D. Rinderknecht, W. L. Popp, J. E. Duarte, O. Lambercy, J. Paik, B. J. Martin, R. Riener, V. Klamroth-Marganska, *Front. Human Neurosci.* **2020**, *14*, 65.